Modelling and molecular dynamics simulation of novel anticancer ligand for restructuring mutant P53 into wild type

Ashik Chhetri and Moloy Roy

Dr. B.C. Roy College of Pharmacy & Allied Health Sciences,
Durgapur-713206, WB, India
Email: ashikchhetri97@gmail.com
Email: 289moloy@gmail.com

Aditi Gangopadhyay and Achintya Saha

Department of Chemical Technology,
University of Calcutta,
Kolkata-700009, WB, India
Email: aig.bioinfo@gmail.com
Email: achintya_saha@yahoo.com

Puja Mishra, Amit Kumar Halder and Souvik Basak*

Dr. B.C. Roy College of Pharmacy & Allied Health Sciences,
Durgapur-713206, WB, India
Email: pujamay12@gmail.com
Email: amitcsir2011@gmail.com
Email: souvik_basak1@yahoo.com
*Corresponding author

Abstract: Mutant p53 is one key factor of cancer or cellular oncogenesis as mutant P53 loses its functions due to the unfolding of its loops, losing its dynamics, DNA-protein interaction, and thus losing its function. Thus, one of the key strategies for developing anti-cancer drugs may be to design leads that can revert mutant P53 to wild type P53. In this regard, we have designed two nitrogen-based heterocyclic ligands that are computationally revealed to revert mutant P53 to wild type. In addition, molecular dynamics simulation revealed a stable complex of the ligands with mutant P53, conformational flexibility of the ligand with the binding cleft and the loop, and structural reversal of the mutant P53 into a protein that mimics wild type P53. We claim this may be the promising lead of broad-spectrum anticancer drugs since it has the potential for functional reversal of mutant P53 in carcinogenic cells.

Keywords: mutant P53; LEA3D; genetic algorithm; molecular dynamics; binding cleft.

Reference to this paper should be made as follows: Chhetri, A., Roy, M., Gangopadhyay, A., Saha, A., Mishra, P., Halder, A.K., and Basak, S. (2022) 'Modelling and molecular dynamics simulation of novel anticancer ligand for restructuring mutant P53 into wild type', *Int. J. Computational Biology and Drug Design*, Vol. 15, No. 2, pp.77–95.

Biographical notes: Ashik Chhetri has completed BPharm from Dr. B. C. Roy College of Pharmacy and Allied Health Sciences, Durgapur in 2020. Currently he is a final year student at National Institute of Pharmaceutical Education and Research, Ahmedabad (NIPER-A) pursuing MS in Medicinal Chemistry, working in the area of organic synthesis focusing on Nickel catalysed selective mono-defluorination for late stage modification of organic compounds utilising 'Green Chemistry' approaches. He is interested in bioinformatics, sustainable synthetic chemistry, transition metal chemistry especially for C-H and C-F activations and development of new reaction strategies for synthesis of novel pharmaceuticals.

Moloy Roy has completed BPharm from Dr. B. C. Roy College of Pharmacy and Allied Health Sciences, Durgapur in 2020, Currently he is a first year student of MPharm in Pharmaceutical Analysis in Dr. B. C. Roy College of Pharmacy and Allied Health Sciences, Durgapur. He has work experience in Disha Eye Hospital as registered clinical pharmacist and in Medclin Research Private Limited as Clinical Research Coordinator (CRC). His research interest is in computational chemistry and various synthetic procedures regarding medicinal agents.

Aditi Gangopadhyay is an Independent Researcher working at the Department of Chemical Technology, University of Calcutta, India. Her areas of interest include computer-aided drug discovery, drug repurposing, infectious diseases, and computational protein structure analysis. She has published 15 research papers in national and international conferences, and authored 4 book chapters. She is also working as a scientific editor at Oxford Science Editing, Oxford, UK.

Achintya Saha, Professor and Ex-Head, Department of Chemical Technology, University of Calcutta, has 28 years of teaching and research experiences. He has published more than 150 research papers and contributed 8 books chapters. He chaired more than 20 national and international conferences. Twenty research scholars awarded PhD under his guidance and presently seven scholars are working under his supervision. He has handled twelve national & international projects, worth INR 3 Cr.

Puja Mishra is pursuing PhD from MAKAUT University, W.B. and have completed MPharm (Pharmaceutical Chemistry) and BPharm from IIT BHU and Institute of Pharmacy, Jalpaiguri, respectively. She has qualified GPAT and NIPERJEE in 2015. Her research interest is in Pharmaceutical Chemistry-Drug design, Docking (Lead modification and optimisation), novel molecule synthesis and their characterisation and in vitro and in vivo studies. Her teaching experience is 4.5 Years and the courses taught are DPharm; BPharm; MPharm. She has guided 2 MPharm and 20 BPharm students. She has been honoured to be a reviewer of *International Journal of Life Science and Pharma Research*. Her research publications include, 5 Full Papers and 2 Book Chapters which sums the cumulative impact factor (as on 2022) to be 9.278.

Amit Kumar Halder is currently working as an Associate Professor in Dr. B. C. Roy College of Pharmacy and Allied Health Sciences, West Bengal, India. He completed his PhD in Pharmacy from Jadavpur University, India in 2016.

As a postdoctoral researcher he worked in University of Kwazulu-Natal, South Africa for one year and University of Porto, Portugal for four years. His specialisation is computational chemistry, synthetic medicinal chemistry and cancer biology. So far, he has authored in more than 50 international publications and has four book chapters.

Souvik Basak is currently working as an Associate Professor in Dr. B. C. Roy College of Pharmacy and Allied Health Sciences, West Bengal, India and acting as Divisional In Charge, Department of Pharmaceutical Chemistry and Pharmaceutical Analysis. He has pursued his BPharm and MPharm from Department of Pharmaceutical Technology, Jadavpur University, Kolkata and Completed his PhD from School of Chemical and Biomedical Engineering, Nanyang Technological University, Singapore. He has published more than 33 papers in various journals of international repute and 6 book chapters. Currently (2022), his cumulative impact factor (SCI) is more than 100 and citations more than 250.

1 Introduction

The International Agency for Research on Cancer (IARC) TP53 database, version R20 (https://p53.iarc.fr/), comprises data of approximately 29,900 somatic mutations of P53. Mutations in P53 lead to the loss of its tumour suppressor function and various missense mutations have been reported in several human cancers, including ovarian serous carcinoma, small cell lung cancer, pancreatic cancer, head and neck squamous cell carcinoma, and invasive breast carcinoma. Therefore, mutations of P53 may be considered to be one of the important causes of breast cancer (Blandino et al., 2018). Various therapeutic strategies, including the suppression of P53 levels by targeting mutant P53 and restoring the activity of wild-type P53, have been attempted. 1-(propoxy methyl)-maleimide (MIRA-1) was developed for specifically targeting mutant P53; however, further investigations were ceased owing to the high toxicity of MIRA-1 (Ozaki and Nakagawara, 2011; Bou-Hanna et al., 2015). PRIMA-1 [2,2 bis-(hydroxymethyl)-3-quinuclidinone] and PRIMA-1 met (methylated PRIMA-1) or APR- 246 binds to mutant p53 and restores its wild type conformation, and are being tested in clinical trial (Perdrix et al., 2017; Zhou et al., 2019; Mantovani et al., 2019). Zinc metallochaperone-1 (ZMC-1) is another small molecule that restores the activity of mutant P53 but has been reported to be highly toxic (Yu et al., 2012; Kogan and Carpizo, 2018). The 2-sulfonypyrimidine compound PK11007 increases thermal stability and specifically inhibits the viability of cancer cell lines expressing mutant P53 and also induces cell death by depleting cellular GSH and increasing the levels of reactive oxygen species (ROS) (Synnott et al., 2018). Although various molecules have been developed for inhibiting mutant P53 and restoring the wild-type activity, several candidates have failed in the clinical trial due to shortcomings, and thus the discovery of such ligands requires further investigations.

2 Experimental

All the proteins structures used in this study were retrieved from the PDB (www.rcsb.org). The structures of the ligands were constructed and optimised in Chem

Office (Perkin Elmer, Waltham, Massachusetts, USA) and ChemSketch (ACD Lab, Toronto, Canada). The 3D structures of the ligands were generated using CORINA (Sadowski and Gasteiger, 1993) and energy minimisation was performed using Avogadro using the steepest descent algorithm and the Universal Force Field (UFF) (Hanwell et al., 2012). The protein structures were tailored and analysed in AutoDock v 4.2 (Scripps Research Institute, La Jolla, California, USA), Discovery Studio Visualizer (Dassault Systems, BIOVIA, San Diego, USA). De novo ligand design was performed using LEA3D (Douguet, 2010; Douguet et al., 2005). MD simulations were performed using Amber 20 (University of California, San Francisco, USA) using GAFF force field.

2.1 Molecular docking

All the docking in the study was performed using AutoDock v4.2. The PDB structure 6GGD, comprising the Y220C mutant P53 was selected as the target. The PDB structure of the peptide was checked in PROCHECK and the model was refined in MODREFINER. Charges on relevant atoms were equilibrated using PDB2PQR using AMBER ff14SB force field. The corresponding charged PQR file was further added with hydrogens, any artefacts were repaired with loop refinement with MODELLER, charge assignments were re-equilibrated with AMBER ff14SB force fields, protonation was done with aspartic acid (the ionisable amino acid within the binding site). Any missing side chains were reconstituted with Dunbrack 2010 rotamer library, hydrogens were added before docking. The prepared protein was processed in AutoDock Tools 4.0 ((The Scripps Research Institute, LaJolla, California) by adding Kollman charges, merging non-polar hydrogen, and removing water molecules. A cubic grid was defined around the binding site of the ligand K9324 in the PDB file 6GGD. The dimensions of the grid along the x, y, and z axes were $50 \times 0 \times 50$, respectively, and the grid spacing was 0.375 Å. The X, Y, and Z coordinates of the grid were 123.508, 105.167, and –44.452, respectively. The ligand was docked flexibly using the Lamarckian genetic algorithm, using 250 runs. The number of generations was 27000 and the number of energy evaluations was set at 2500000. The rate of gene mutation was 0.02 and the crossover rate was 0.8. For studying convergence, the docked solutions were clustered using a clustering RMSD of 2.0 Å, and the lowest-scoring pose of the largest cluster was selected as the optimum solution. The binding affinity was reported in Gibb's free energy (ΔG) format and the binding interactions were determined using Discovery Studio Visualizer 3.5.

2.2 De novo ligand design

De novo ligand design was performed using fragment-based library design and genetic algorithm method. Briefly, ligand PK9324 (PDB ID: EYB) was chosen as a template and optimised in LEA3D. The template is dissected, hybridised with 7986 drug-like fragments, docked in situ with PLANT algorithm, multiplied with thirty rounds of screening and mutational crossing over was allowed for each round. Out of 18 non-redundant elucidated candidates, best (De1) was chosen based on fitting function evolved as a weighted average of PLANTS and FlexX based docking algorithm.

2.3 Molecular dynamics simulations

The protonation states of amino acid residues of the protein complexes were fixed at pH = 7.0 with the help of by the PDB2PQR server (http://server.poissonboltzmann.org/pdb2pqr, accessed on 12 February 2022), using the AMBER forcefield and output naming scheme (Dolinsky et al., 2007). The ff99SB and the general AMBER force field (GAFF) were used for describing receptor-ligand and ligand–water interactions, respectively (Wang et al., 2004). The ligand parameterisations were subsequently carried out with Leap implemented in Amber 20 under general AMBER force field (GAFF) in Antechamber (Case et al., 2020). MD simulations were performed with the ff99SB force field with the TIP3P explicit water in a cubic box with 8Å distance around the protein complexes. Subsequently, the positive charge of the all complexes was neutralised by chloride ions. Partial Mesh Ewald (PME) method was used to consider long-range electrostatic forces (cutoff of 12 Å). Additionally, the SHAKE algorithm was used to constrain all bonds. Energy minimisation was performed in two stages to reduce the bad clashes of the atoms of initially prepared solvated complexes. In the first stage, only ions and water molecules were relaxed by 2000 step minimisation process (1000 steps of steepest decent minimisation followed by 1000 of conjugated gradient) by employing a restrained force of 500 kcal/mol on the solute. In the second stage, the whole system was relaxed by 5000 step minimisation process (2500 steps of steepest decent minimisation followed by 2500 of conjugated gradient). The minimised system was gradually heated up from 0 K to 300 K with a weak harmonic restraint of 10 kcal/mol to keep the solute fixed for 200 ps. Subsequently, the 2-ns constant pressure equilibration at 300 K was performed. Finally, the 50-ns MD simulations without restriction were run with constant temperature (300 K) and constant pressure (1 atm) (Halder and Honarparvar, 2019; Halder and Cordeiro, 2021).

After completion of simulation, post-dynamics analysis over the MD trajectories was performed using PTRAJ and CPPTRAJ module (Roe et al., 2013) implemented in Amber20 to analyse the root mean square deviation (RMSD), root mean square fluctuatuion (RMSF), radiation of gyration and hydrogen bond.

Molecular Mechanics Generalised Born Surface Area (MM-GBSA) (Srinivasan et al., 1998; Ylilauri et al., 2013) binding free energies of PIs were calculated using MM-PBSA program in Amber20 where one hundred snapshots were taken from the last 10 ns of MD trajectory. The binding energy calculation is represented as the following equation:

$$\Delta G = \Delta E_{\text{ele}} + \Delta E_{\text{vdW}} + \Delta G_{\text{pol}} + \Delta G_{\text{nonpolar}} - T\Delta S$$

ΔE_{ele} and ΔE_{vdW} represent electrostatic and van der Waals interactions between the ligands and the proteins in gas phase), respectively. The polar and non-polar solvation free energies are represented by ΔG_{pol} and $\Delta G_{\text{nonpolar}}$, respectively. The entropy contributions ($-T\Delta S$) of the binding free energies were calculated using normal mode analysis for the complexes from changes in the translational, rotational, and vibrational entropy components by taking 400 snapshopts in last 10-ns simulation. Finally, the entropy contribution ($-T\Delta S$) of the binding free energies were calculated using normal mode analyses taking 100 snapshots from the last 10 ns of the MD trajectory(Halder and Honarparvar, 2019).

2.4 Structure-based pharmacophore mapping

The structure-based pharmacophores were developed with recently developed open-access Python tool named OpenPharmacophore which is available at https://github.com/uibcdf/OpenPharmacophore. OpenPharmacophore is able to generate structure-based pharmacophore from the ligand bound structures submitted in.pdb formats. In the current work the following parameters – radius:1 and hydrophobics: PLIP. After generating the pharmacophores these were saved as.jason formats that were imported in Zinc-Pharmer (Koes and Camacho, 2012) webserver to align the ligands with these structure-based pharmacophores.

2.5 Evaluation of drug-likeliness and toxicity profile of compounds

The drug-likeliness of the selected ligands was evaluated by predicting the number of violations of Lipinski's rule of five, using the Molinspiration (https://www.molinspiration.com/cgi-bin/properties). In silico toxicity, the prediction was performed using the SwissADME. The structures of the ligands were converted to SMILES format and were used as the input for the Molinspiration and SwissADME servers.

3 Results and discussion

3.1 De novo ligand design

De novo ligand design is an effective strategy for optimisation of leads to more effective scaffolds, in which the template ligand is manipulated in the active site. In this study, we used thirty rounds of screening in eLEA3D, based on the Protein-Ligand ANT (PLANT) algorithm, and obtained 18 different ligands**.** The ligands were re-docked to the binding site of 6GGD using AutoDock v 4.2 and found that the binding affinities of ligands 1, 10, 11, 13, 14, 17, and 18 were the highest (Table 1). Interestingly, the compounds with the highest binding affinities possessed pyridine and/or pyrazole rings.

3.2 Hit selection

For hit selection, a binding affinity of more than –8.5 kcal/mole and interactions with the mutation site were the two necessary criteria. Ligands 1, 10, 11, 13, 14, 17, and 18 satisfied the former criteria and had considerably high binding affinities (Table 1). Ligands 1 and 14 satisfied both the criteria, with binding affinities of –8.6 and –8.9 kcal/mol, respectively, and interacted with the mutation site. We, therefore, selected ligands 1 and 14 as hits against the mutant P53 protein, 6GGD, by de novo and docking-based ligand design. Moreover, binding site analysis revealed that both the ligands interacted with the most vulnerable mutation zone in P53 (residues 128 to 285) (Figure 1). Ligands 1 has been designated as De1 in our study. De1 interacted with the mutant P53 (6GGD)via several common binding residues, including C220 (Y220C mutation in P53), V147, L145, T230, P223, T150, and P153. The designed compound was revealed to cover the mutation point of the taken mutant P53(Y220C) and also the hotspot of mutation (residue 128 to 285 for mutant P53, collected from TP53database, https://p53.iarc.fr/) (Figure 1).

Table 1 Binding affinities of de novo designed ligands

Ligand annotation	*Binding affinity* (Kcal/mol)
Lig1	–8.6
Lig2	–7.5
Lig3	–7.2
Lig4	–8.4
Lig5	–7.5
Lig6	–7.9
Lig7	–6.6
Lig8	–6.3
Lig9	–6.3
Lig10	–8.8
Lig11	–8.7
Lig12	–7.5
Lig13	–9.0
Lig14	–8.9
Lig15	–7.4
Lig16	–6.3
Lig17	–8.0
Lig18	–9.5

Figure 1 Binding interactions of DE1 with Y220C mutant P53 (PDB id: 6GGD) (see online version for colours)

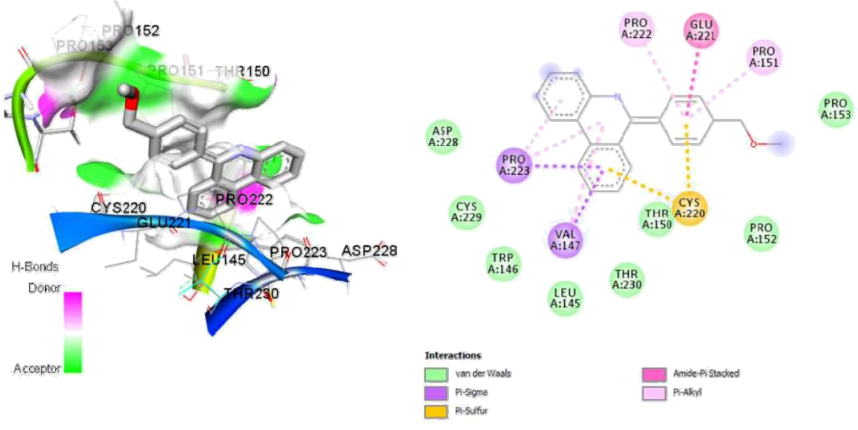

3.3 Molecular dynamics simulation

3.3.1 Molecular docking

The 250 docked solutions were clustered by a cut-off RMSD of 2.0 Å. The 250 docked solutions for compound De1 formed 2 clusters, of which the smaller cluster comprised 103 solutions and the larger cluster comprised 147 solutions. Although the convergence was not ideal for De1, the smaller cluster comprised 103 solutions, and the binding

energy was –9.76 kcal/mol. The ligand the efficiency value of this solution was –0.42. The lowest scoring pose of the smaller cluster was selected as the optimum docked solution, as it represented the lowest scoring pose of the entire run, and the energy difference between the two clusters was 0.33 kcal/mol.

3.3.2 Stability of the complex formed by de1

The docked pose of the De1 (named as 6GGD-De1 complex) with Y220C mutant P53 (PDB: 6GGD) was used for 50 ns explicit solvent MD simulation analyses to understand the dynamic behaviour of this protein complex. For comparative analyses, two other complexes were subjected to the same 50 ns MD simulations. The first complex, which is named 6GGD- PK9324, consisted of the bound ligand of 6GGD that was reported with the name PK9324 in the original investigation where this protein was reported. The second complex (named as 6GGD-PK9318), one other hand, contained another ligand named PK9318. Note that the complex of PK9318 with Y220C mutant P53 is found in the Protein Data Bank with id 6GGB (Bauer et al., 2019). The structures of 6GGB and 6GGD as well as bioactive conformations of their bound ligands (i.e., PK9318 and PK9324) are superimposable and the bioactive conformation of PK9318 was thus directly extracted from 6GGB and was subsequently complexed with 6GGD structure for MD simulation analyses. It is also noteworthy that both PK9318 and PK9324 were previously reported as small-molecule stabilisers against Y220C mutant P53 with differential scanning fluorimetry ΔT_m values of 3.6°C and 1.8°C indicating the former as a better stabiliser. Furthermore, PK9318 was also reported with Isothermal titration calorimetry (ITC) Kd value of 2.4 μM. Therefore, complexes with these two ligands may serve as references for analysing the dynamic behaviours of the designed ligand De1.

The RMSD plots of three complexes were first observed and it is presented in Figure 2 it is evident that the 6GGD-De1 complex depicted similar fluctuations as compared to 6GGD-PK9318 as both these complexes were stabilised after 10 ns. These two complexes consistently displayed RMSDs of 2.5Å in 50 ns run. However, the 6GGD-PK9324 complex was stabilised after 30 ns. The average RMSD values of 6GGD-De1, 6GGD-PK9318, and 6GGD-PK9324 are 1.56 Å, 1.59 Å, and 1.81 Å, respectively. Similarly, the fluctuations of the ligands in the complexes at the binding site were also inspected by observing their RMSDs (i.e., ligand RMSD) that demonstrated that all these ligands were stabilised at their initial binding sites since RMSDs of all these bound ligands were found to be less than 2.0 Å. However, it may also be inferred that the ligands of 6GGD-De1 and 6GGD-PK9318 displayed slightly better stabilities as compared to that of 6GGD-PK9324.

Furthermore, we also studied RMSF and radiation of gyration plots of these three complexes that are shown in Figure 3. The RMSF plots of the proteins suggested that the binding behaviour of De1 is more similar to the PK9318 as compared to PK9324. On the other hand, the radiation of gyrations plots indicated sufficient rigidity of all these three complexes.

After confirming the binding stability of De1 from trajectory analyses we performed MMGBSA analyses with all these three complexes and the results of these analyses are shown in Table 2.

Figure 2 RMSD plots of (A) protein complexes and (B) bound/docked ligands in 50 ns MD simulations (see online version for colours)

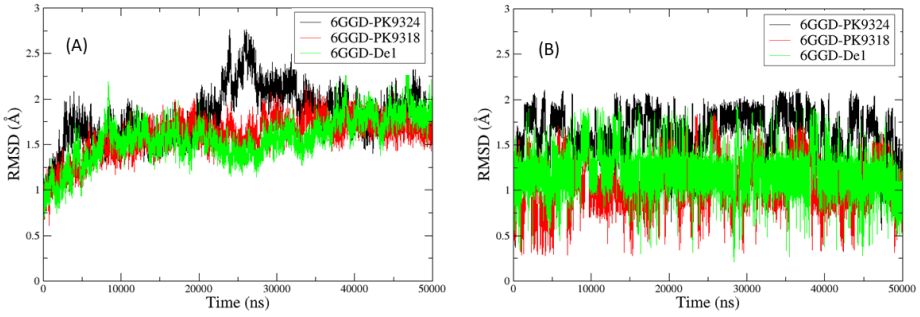

Figure 3 Plots of (A) RMSF and (B) radiation of gyration of protein complexes in 50 ns MD simulations (see online version for colours)

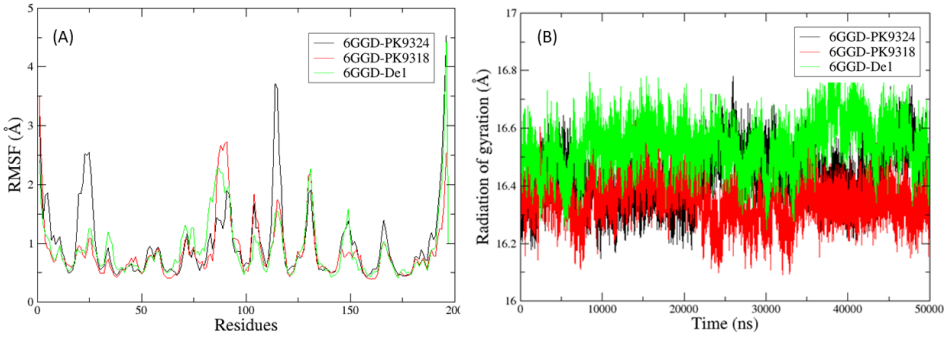

Table 2 Calculated binding free energies [$\Delta G_{bind}(T)$] of the complexes. The energy components are in kilocalories per mole

Complexes	ΔE_{vdW}	ΔE_{elec}	ΔG_{gas}	ΔG_{polar}	$\Delta G_{nonpolar}$	$\Delta G_{solvation}$	$-T\Delta S$	$\Delta G_{bind}(T)$
6GGD-PK9324	–44.39	–100.49	–144.88	112.27	–4.75	107.52	–23.16	–14.20
6GGB_PK9318	–44.86	–113.16	–158.02	124.54	–4.87	119.66	–18.22	–20.14
6GGD_De1	–41.97	–5.44	–47.42	13.05	–4.77	8.28	–22.64	–16.50

The theoretical binding energy ($\Delta G_{bind}(T)$) of PK9318 in the 6GGD-PK9318 complex was found to be higher than PK9324 in the 6GGD-PK9324 complex and it complies with their experimental data as described previously. Interestingly, $\Delta G_{bind}(T)$ of De1 complex was found to be higher than PK9324 but lower than PK9318. Nevertheless, these theoretical values imply that the De1 may indeed be projected as a potential inhibitor of the Y220C mutant P53. Additionally, it is also observed that De1 is likely to demonstrate binding interactions that are significantly different from both PK9318 and PK9324. Note that it was also insinuated from the docked pose of the De1 (shown in Figure 1). The van der Waals interactions of this compound are similar to the other two ligands but it is

likely to depict much fewer electrostatic interactions with the receptor that was also obtained from the docked structure. However, low electrostatic interactions of De1 may be compensated with solvation-free energy that significantly improved its overall ΔG_{bind}. However, such differences in binding interactions are not unexpected from the ligand that was designed by *de novo* ligand design but more importantly this designed ligand displays sufficient binding stability in its protein complex and its binding energy is also comparable to the binding energies of experimentally tested ligands (i.e., PK9318 and PK9324). To further understand how De1 may interact with the binding site amino acid residues, per residue decomposition analysis was performed with 6GGD-De1 complex and the interactions are depicted in Figure 4.

Figure 4 Per-residue decomposition profiles of the De1 complex with Y220C mutant P53 (see online version for colours)

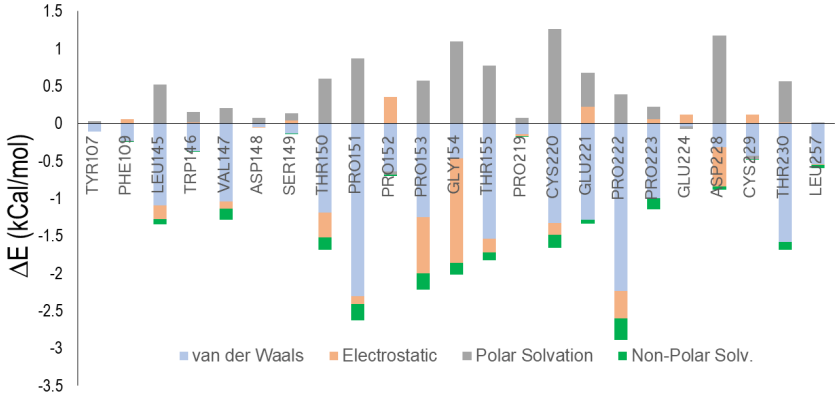

In Figure 4, it is observed that De1 was able to make van der Waals interactions with most of its surrounding amino acids during MD simulation. However, electrostatic interactions were observed with some selected amino acid residues such as Thr15, Pro153, and Gly154 though the interactions with Gly154 residue were more prominent. Even though the polar interactions with Gly150 are not observed in the docked pose of De1, in the long MD run these polar interactions may become vital for the stability of its complex. To confirm this hydrogen bond analyses were performed and it was observed that almost 50% of frames of the 6GGD-De1 complex were associated with the hydrogen bond interactions between Gly154 residue and De1.

The RMSD values of the protein backbone and ligand is represented in Figure 5. The high RMSD values of De1 could be attributed to the torsional flexibility around the C7-C8, C11-C12, and C12-O13 bonds, as observed in the ligand torsion profile (Figure 5). The torsional flexibility around the C11-C12 and C12-O13 bonds was higher than that around the C7-C8 bond, which could be attributed to the fact that the flexibility of the C7-C8 bond was restricted by the two bulky aromatic groups on either side. The values of molecular surface area (Mol SA), solvent accessible surface area (SASA), and polar surface area (PSA) of De1 remained steady throughout the simulation, and are depicted in Figure 6.

Figure 5 (a) Radial plots depicting the torsional profile of De1 during the 50 ns simulation. The torsional conformations of the C11-C12 and C12-O13 bonds are represented in green and blue, respectively, and were lesser than that around the C7-C8 bond, represented in red. (b) The 2D structure of De1 showing the rotatable bonds in the corresponding colours in (a) (see online version for colours)

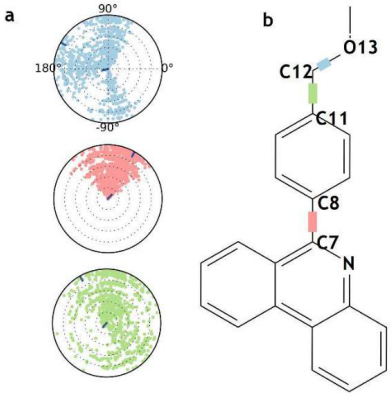

Figure 6 Values of the molecular surface area (MolSA), solvent accessible surface area (SASA), and polar surface area (PSA) of De1 over the 50 ns trajectory (see online version for colours)

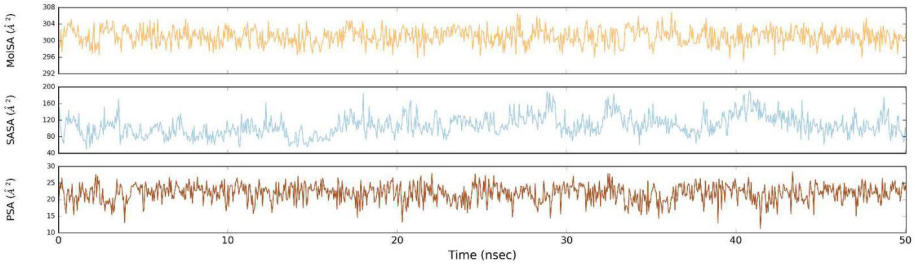

3.4 Structure based pharmacophore mapping

Realising the difference between the receptor binding mechanisms of bound ligands De1 with the protein, we finally performed structure-based pharmacophore mapping with their receptor-bound structures. The results are depicted in Figure 7. It is observed that the pharmacophores of both the PK9324 and De1 have four pharmacophore features consisting of three hydrophobic (H) and one hydrogen bond donor (D) features. However, as evident from Figure 7, the orientations of these pharmacophores in 3D space are different. Nevertheless, when we fitted docked ligand De1 with the structure-based pharmacophore generated with bound ligand PK9324, De1 mapped with three hydrophobic pharmacophoric features. Similarly, when PK9324 was mapped against structure-based pharmacophore constructed with docked De1, the former also fitted with three hydrophobic features. Therefore, even though different mechanisms may be followed by the designed ligand as compared to PK9324, these two compounds may have common pharmacophoric features.

Figure 7 Structure based pharmacophores developed with (I) bound-ligand PK9324 and (II) docked ligand De1 (D: Hydrogen bond donor, H: Hydrogen bond acceptor) (see online version for colours)

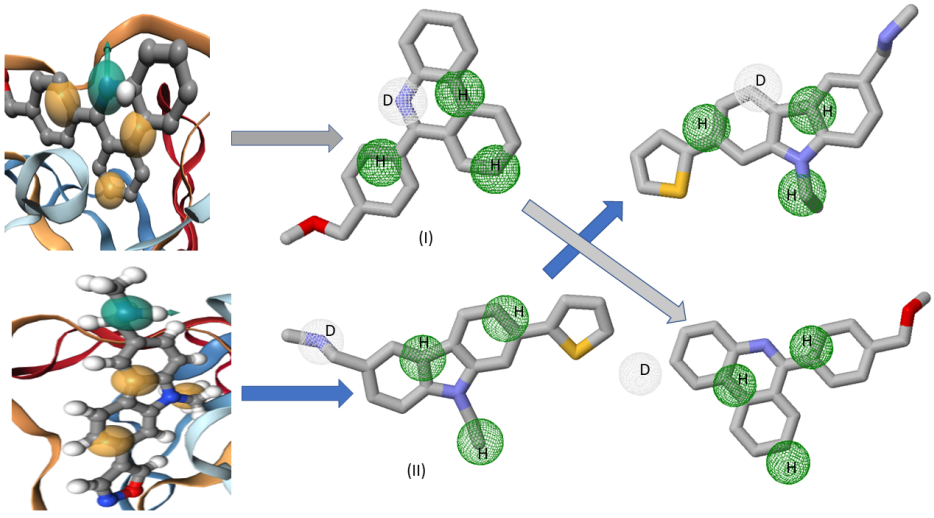

3.5 Structural alteration of mutant P53 on ligand binding

Now, the question lies can De1 alter the conformation of Y220C mutant P53 and lead to reversal of function of mutant P53 to WT P53? Y220 falls within the DNA binding domain, which is mediates the formation of electrostatic interactions with V147, P151, P153, and P223, P222 residues located on the S3/S4 and S7/S8 loops (Md et al., 2013). Mutations of Y220, such as the Y220C mutation, disrupts these interactions and destabilises the loops, especially S7/S8. The substitution of the tyrosine to a cysteine enlarges the hydrophobic pocket at this region by conjoining the two preexisting hydrophobic cores in this region into an elongated beta crevice which leads to the exposure of several hydrophobic residues including L145 to the solvent (Ferreira et al., 2018). This destabilises P53 by lowering its melting temperature (Tm) by approximately 7–8ºC, which subsequently leads to unfolding, aggregation, and inactivation of P53 (Bullock et al., 2000; Wang and Fersht, 2017). A further investigation on anatomy of hydrophobic cleft in between S3/S4 and S7/S8 proximal loops of 6GGD, revealed that De1 (Figure 8) align themselves in the hydrophobic cavity in Y220C mutant in such a way that the side chain of C220 rotates itself towards the ligands instead of the hydrophobic cavity of the protein. Hence, we hypothesise that the elongated hydrophobic cleft as described earlier (Figure 8(a)) (Joerger et al., 2015) due to Y220C mutation may be shortened by De1 (Figure 8(b)) helping further to reform the S3/S4 and S7/S8 interactions. The further overlap of PK9324-6GGD and De1-6GGD induced hydrophobic pockets (Figure 9) with proximal dipole moments also suggests the similar reprogramming of mutant P53 structure into wild type as reported earlier (Bauer et al., 2016, 2020; Baud et al., 2018).

Figure 8 Re-orientation of the hydrophobic cleft within 6GGD in between S3/S4 and S7/S8 loops after De1 binding. (a) Hydrophobic cleft in Y220C mutant before ligand binding. (b) Hydrophobic cleft in Y220C mutant after ligand binding (see online version for colours)

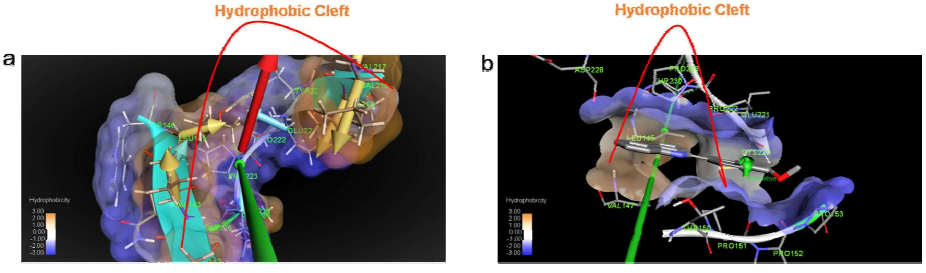

Figure 9 Overlap of PK9324-6GGD and De1-6GGD. The golden one is the PK9324 bound with the protein while the normal one is the De1 bound with the same protein (see online version for colours)

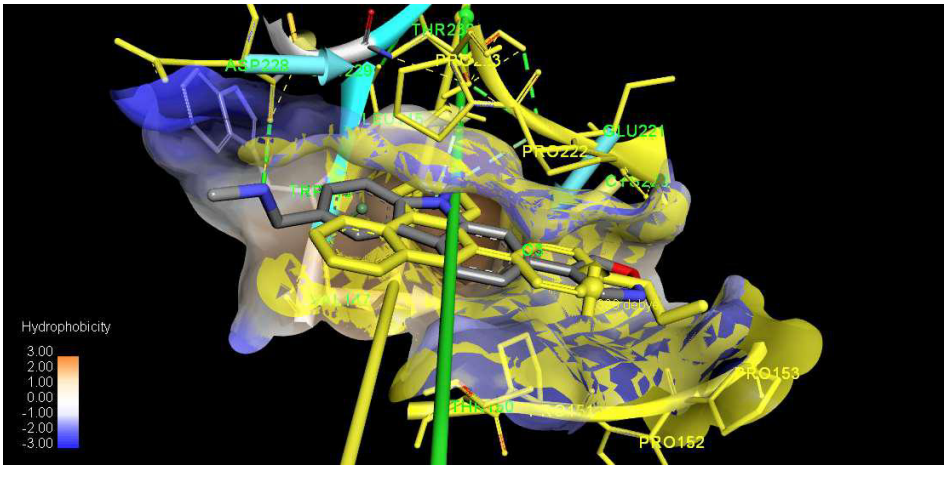

3.6 Drug-likeliness screening

Prediction of drug-likeliness properties of the compounds using Molinspiration revealed that the molecules obeyed Lipinski's Rule of Five, except the log P values. The molecular weight of the compounds ranged from 342 to 442, the number of hydrogen bond donors (nOHNH) was 0 or 1, and the number of hydrogen bond acceptors (nON) ranged from 2 to 6. However, the log P values of the compounds ranged from 6.01 to 6.39 and exceeded the permissible value of ≤5.0. The number of rotatable bonds was 4. The drug-likeliness properties of the compounds are enlisted in Table 3. Although De1 showed moderate inhibition of some endogenous receptor in human, it has shown promising safe profiles such as non-binding to various liver microsomal enzymes such as CYP2C9 or CYP2D6 or CYP3A4, improved cell permeation as demonstrated by improved Caco-2 cell permeability, null carcinogenicity and others (Table 4).

Table 3 Lipinsky's Rule evaluation of selected ligands

Lipinsky's regimen	*De1*
miLogP	6.39
TPSA	22.13
natoms	26
MW	341.4
nON	2
nOHNH	0
nviolations	1
nrotablebonds	4
Volume	331.2

Table 4 *In silico* toxicity prediction by admetSAR

Ames mutagenesis	+
Acute Oral Toxicity (c)	III
Androgen receptor binding	+
Aromatase binding	+
Avian toxicity	–
Blood Brain Barrier	+
BRCP inhibitor	–
Biodegradation	–
BSEP inhibitor	+
Caco–2	+
Carcinogenicity (binary)	–
Carcinogenicity (trinary)	Non-required
Crustacea aquatic toxicity	+
CYP1A2 inhibition	+
CYP2C19 inhibition	+
CYP2C9 inhibition	–
CYP2C9 substrate	–
CYP2D6 inhibition	–
CYP2D6 substrate	–
CYP3A4 inhibition	–
CYP3A4 substrate	+
CYP inhibitory promiscuity	+
Eye corrosion	–
Eye irritation	–
Estrogen receptor binding	+
Fish aquatic toxicity	–
Glucocorticoid receptor binding	+

Table 4 *In silico* toxicity prediction by admetSAR (continued)

Honey bee toxicity	+
Hepatotoxicity	+
Human either-a-go-go inhibition	+
Human Intestinal Absorption	+
Human oral bioavailability	–
MATE1 inhibitor	–
Micronuclear	–
Acute Oral Toxicity	2.50140738
OATP1B1 inhibitor	+
OATP1B3 inhibitor	+
OATP2B1 inhibitor	–
OCT1 inhibitor	+
OCT2 inhibitor	–
P-glycoprotein inhibitor	+
P-glycoprotein substrate	–
PPAR gamma	+
Plasma protein binding	1.12477338
Subcellular localisation	Mitochondria
Tetrahymena pyriformis	1.33994842
Thyroid receptor binding	+
UGT catalysed	–
Water solubility	–3.35608998

4 Discussion

The Compound De1 showed considerable binding affinity with 6GGD in the binding pocket revealing that the compound possesses significant point of contacts with the receptor cavity. The de novo designed ligand thus suggests successful construction of scaffold and subsequent optimisation through crossing over (genetic algorithm) to define newer molecule covering Y220C point of mutation in mutant P53. Molecular dynamics simulation revealed that the compound fits in the binding pocket with stability and it matches with a good fit ligand PK9318 which has been reported as a stabiliser of mutant P53 (Y220C). This stabilisation potential of De1 may be attributed either to its multiple interactions with the 6GGD or its lower solvation energy (ΔGsolvation) which has led to its easy displacement of binding site water molecules and sitting inside the binding cavity. Interestingly, the binding energy of De1 has been found higher under AMBER force field compared to PK9324, the inbound ligand to the same Y220C mutant and comparable to that of PK9318, the ligand with the best binding affinity reported by the same group of authors against 6GGD. Furthermore, the RMSF of the ligand-protein complex showed lesser deviation than PK9324-6GGD complex and comparable to PK9318-6GGD suggesting stable binding of the ligand inside the complex.

To understand the stable seating of De1 inside the binding cavity, we analysed the conformational flexibility of De1 during MD run through radial plot of torsional angles of various bonds inside the same. The further dissection revealed that the bonds C11-C12 as well as C12-O13 have remained flexible during De1 binding with the mutant protein. Thus it may be presumed that the degree of freedom of such bonds' rotation have originated suitable conformers of De1 that may nicely seat into the binding pocket of 6GGD. The polar and solvent accessible surface area of De1 remained steady throughout the simulation suggesting exposure of the same hydrophilic and hydrophobic surfaces of the same during the entire run. This corroborate our hypothesis that De1 assembles with the 6GGD in a favoured binding mode thus suggesting that De1 may be a steady inhibitor of Y220C mutant P53.

The De1 further have displayed reduction of the hydrophobic cavity of Y220C mutant P53 resulting in proximation of S3/S4 and S7/S8 loops which may restore the polar electrostatic interactions between the confronting amino acids of the counterfacing loops. Thus, it may regain the folding conformation of P53 enabling it to act as oncho-suppressant in spite of having mutation within its domain. Basically, the most detrimental effect of P53 mutation is the loss of its beneficial function of cell cycle regulation which is basically due to loss of its folded conformation owing to mutation. Although the mutant P53 could be targeted to destroy by organic inhibitors resulting in population supremacy of wild type (WT) P53 (which could rule the cell cycle or cell proliferation), the target non-specificity of such inhibitors could co-damage the WT P53 together with the mutant ones. Hence, the alternative method to restore the functional loss of mutant P53 could be a promising strategy to combat cancer (Joerger et al., 2015; Bauer et al., 2016, 2020; Baud et al., 2018) which is achieved in our designed lead with plausible approximation. Although the synthesis and evaluation of the De1 is still under process in our lab, we propose that it possess a good pharmacophore similarity with carbazole derivatives that have been proved to reverse mutant P53 into WT ones in earlier works (Joerger et al., 2015; Bauer et al., 2016, 2020; Baud et al., 2018; Gomes et al., 2021) where the authors tried carbazole or carbathiazole derivatives experimentally on mutant P53 and reported considerable gain of function. Our ligand possesses similar pharmacophore, only the azole or thiazole of the reported ones' has been substituted by azine. It has also heteroatomic or structural resemblance with the co-crystallised or designed ligands published elsewhere (Gomes et al., 2021; Radhakrishnan et al., 2021) that are reported to be experimentally proven as mutant P53 inhibitors/revertant compounds. Thus, we plausibly assume that De1 may revert the loss of function of mutant P53 in the same way when would be experimentally tried against the latter.

The structure-based pharmacophore mapping showed considerable resemblance of De1 with PK9324 or PK9318. Moreover, the mapping also revealed the sanctity of three hydrophobic pockets inside the compound that should be kept intact during designing of the lead. Lastly, it could not be denied that admetSAR analysis revealed some toxic or contra-indicating properties of De1, however, we propose that on further scaffold optimisation o De1 these toxicities may be minimised. For example, De1 showed potentially non-inhibition to the variants of cytochrome P450 in the liver microsome and showed good Caco-2 cell permeability suggesting better absorption from the intestine. It also showed non-carcinogenic indication in admetSAR. The improved P-glycoprotein inhibition is a suggestion of good cell accumulation of the compound. Thus, it may be considered that De1 is a promising ligand to restore lost function mutant P53 into WT

one and further tailoring of the same would make it an alternate lead for anticancer drug design.

5 Conclusion

Thus the De1-mutant P53 (Y220C) interaction revealed that the binding potentials, hydrogen bonds, and other interactions with surrounding amino acids with the main and sub-binding sites were stable. This reprogrammed the orientations of the interacting amino acids, which subsequently reduced the volume of the hydrophobic cleft, reoriented the dipole moment, reestablished the interactions between the S3/S4 and S7/S8 loops, and restored the conformation of the mutant P53 towards WT P53 domain conformation and dynamics. Flexible docking combined with MD simulations further revealed that the ligands fitted properly with the binding site, in terms of flexibility of the residues sheathing the pocket and torsional flexibility surrounding certain bonds surpassing the steric clashes of the bulkier groups present within themselves. Thus the ligand De1 may have the potential of a lead for structural reversal of mutant P53 and thus suppressing cancer.

Conflict of interest

There is no conflict of interest in this manuscript.

References

Baud, M.G.J., Bauer, M.R., Verduci, L., Dingler, F.A., Patel, K.J., Roy, D.H., Joerger, A.C. and Fersht, A.R. (2018) 'Aminobenzothiazole derivatives stabilize the thermolabile p53 cancer mutant Y220C and show anticancer activity in p53-Y220C cell lines', *Eur J. Med Chem.*, Vol. 52, pp.101–114.

Bauer, M.R., Jones, R.N., Baud, M.G., Wilcken, R., Boeckler, F.M., Fersht, A.R., Joerger, A.C. and Spencer, J. (2016) 'Harnessing fluorine-sulfur contacts and multipolar interactions for the design of p53 mutant Y220C rescue drugs', *ACS Chem. Biol*., Vol. 11, pp.2265−2274.

Bauer, M.R., Jones, R.N., Tareque, R.K., Springett, B., Dingler, F.A., Verduci, L., Patel, K.J., Fersht, A.R. and Joerger, A.C. and Spencer, J. (2019) 'A structure-guided molecular chaperone approach for restoring the transcriptional activity of the p53 cancer mutant Y220C', *Future Med Chem.*, Vol. 11, No. 19, pp.2491–2504.

Bauer, M.R., Kramer, A., Settani, G., Jones, R.N., Ni, X., Tareque, R.K., Fersht, A.R., Spencer, J. and Joerger, A.C. (2020) 'Targeting cavity-creating p53 cancer mutations with small molecule stabilizers: the Y220X paradigm', *ACS Chm. Biol*., Vol. 15, pp.657–668.

Blandino, G. and Di Agostino, S. (2018) 'New therapeutic strategies to treat human cancers expressing mutant p53 proteins', *J. Exp Clin Cancer Res.*, Vol. 37, No. 1, p.30.

Bou-Hanna, C., Jarry, A., Lode, L., Schmitz, I., Schulze-Ostoff, K., Kury, S., Bezieau, S. and Mosnier, J-F. (2015) 'Acute cytotoxicity of MIRA-1/NSC19630, a mutant p53-reactivating small molecule, against human normal and cancer cells via a caspase-9-dependent apoptosis', *Cancer Letters*, Vol. 359, No. 2, pp.211–217.

Bullock, A.N., Henckel, J. and Fersht, A.R. (2000) 'Quantitative analysis of residual folding and DNA binding in mutant p53 core domain: definition of mutant states for rescue in cancer therapy', *Oncogene*, Vol. 19, pp.1245−1256.

Case, D.A., K.B., Ben-Shalom, I.Y., Brozell, S.R., Cerutti, D.S., Cheatham III, T.E., Cruzeiro, V.W.D., Darden, T.A., R.E. D., Giambasu, G., Gilson, M.K., Gohlke, H., Goetz, A.W., Harris, R., Izadi, S., Izmailov, S.A., Kasavajhala, K., Kovalenko, A., Krasny, R., Kurtzman, T., Lee, T.S., LeGrand S., Li, P., Lin, C., Liu, J., Luchko, T.R.L., Man, V., Merz, K.M., Miao, Y., Mikhailovskii, O., Monard, G., Nguyen, H., Onufriev, A.F., Pan, S.P., Qi, R., Roe, D.R., Roitberg, A., Sagui, C., Schott-Verdugo, S., Shen, J., Simmerling, C.L.N.R., Skrynnikov, J.S., Swails, J., Walker, R.C., Wang, J., Wilson, L., Wolf, R.M., Wu, X., Xiong, Y., Xue, Y., York, D.M. and Kollman, P.A. (2020) *Amber 2019*, University of California, San Francisco.

Dolinsky, T.J., Czodrowski, P., Li, H., Nielsen, J.E., Jensen, J.H., Klebe, G. and Baker, N.A. (2007) 'PDB2PQR: expanding and upgrading automated preparation of biomolecular structures for molecular simulations', *Nucleic Acids Research*, Vol. 35, Web Server, pp.W522–W525.

Douguet, D. (2010) 'e-lEA3D: a computational-aided drug design web server', *Nucleic Acids Res*., Vol. 38, Web Server issue, pp.W615–W621.

Douguet, D., Munier-Lehmann, H., Labesse, G. and Pochet, S. (2005) 'LEA3D: a computer-aided ligand design for structure-based drug design', *Journal of Medicinal Chemistry*, Vol. 48, No. 7, pp.2457–2468.

Ferreira, S.B., Dantas, T.B., de Figuerêdo Silva, D., Ferreira, P.B., de Melo, T.R. and de Oliveira Lima, E. (2018) 'In silico and in vitro investigation of the antifungal activity of isoeugenol against penicillium citrinum', *Curr Top Med Chem.*, Vol. 18, No. 25, pp.2186–2196.

Gomes, A.S., Ramos, H., Inga, A., Sousa, E. and Saraiva, L. (2021) 'Structural and drug targeting insights on mutant p53', *Cancers*, Vol. 13, No. 3344.

Halder, A.K. and Cordeiro, M.N.D.S. (2021) 'Multi-target in silico prediction of inhibitors for mitogen-activated protein kinase-interacting kinases', *Biomolecules*, Vol. 11, No. 11.

Halder, A.K. and Honarparvar, B. (2019) 'Molecular alteration in drug susceptibility against subtype B and C-SA HIV-1 proteases: MD study', *Structural Chemistry*, Vol. 30, No. 5, pp.1715–1727.

Hanwell, M.D., Curtis, D.E., Lonie, D.C., Vandermeersch, T., Zurek, E. and Hutchison, G.R. (2012) 'Avogadro: An advanced semantic chemical editor, visualization, and analysis platform', *J. Cheminform.*, Vol. 4, p.17.

Joerger, A.C., Bauer, M.R., Wilcken, R., Baud, M.G., Harbrecht, H., Exner, T.E., Boeckler, F.M., Spencer, J. and Fersht, A.R. (2015) 'Exploiting transient protein states for the design of small-molecule stabilizers of mutant p53', *Structure*, Vol. 23, pp.2246−2255.

Koes, D.R. and Camacho, C.J. (2012) 'ZINCPharmer: Pharmacophore search of the ZINC database', *Nucleic Acids Research*, Vol. 40, No. W1, pp.W409–W414.

Kogan, S. and Carpizo, D.R. (2018) 'Zinc metallochaperones as mutant p53 reactivators: a new paradigm in cancer therapeutics', *Cancers*, Vol. 10, No. 6, p.166.

Mantovani, F., Collavin, L. and Del Sal, G. (2019) 'Mutant p53 as a guardian of the cancer cell', *Cell Death and Differentiation*, Vol. 26, No. 2, pp.199–212.

Md, S., Rauf, A., Endou, A., Takaba, H. and Miyamoto, A. (2013) 'Effect of Y220C mutation on p53 and its rescue mechanism: a computer chemistry approach', *Protein J*, Vol. 32, pp.68–74.

Ozaki, T. and Nakagawara, A. (2011) 'Role of p53 in cell death and human cancers', *Cancers* (*Basel*), Vol. 3, No. 1, pp.994–1013.

Perdrix, A., Najem, A., Saussez, S., Awada, A., Journe, F., Ghanem, G. and Krayem, M. (2017) 'PRIMA-1 and PRIMA-1Met (APR-246) from mutant/Wild type p53 reactivation to unexpected mechanisms underlying their potent anti-tumor effect in combinatorial therapies', *Cancers*, Vol. 9, No. 12, p.172.

Radhakrishnan, N., Dhanjal, J.K., Sari, A.N., Ishida, Y., Terao, K., Kaul, S.C., Sundar, D. and Wadhwa, R. (2021) 'Caffeic acid phenethyl ester (CAPE) confers wild type p53 function in p53Y220C mutant: bioinformatics and experimental evidence', *Discover Oncol*., Vol. 12, p.64.

Roe, D.R. and Cheatham 3rd, T.E. (2013) 'PTRAJ and CPPTRAJ: software for processing and analysis of molecular dynamics trajectory data', *J. Chem Theory Comput*., Vol. 9, No. 7, pp.3084–3095.

Sadowski, J. and Gasteiger, J. (1993) 'From atoms and bonds to three-dimensional atomic coordinates: automatic model builders', *Chemical Reviews*, Vol. 93, No. 7, pp.2567–2581.

Srinivasan, J., Miller, J., Kollman, P.A. and Case, D.A. (1998) 'Continuum solvent studies of the stability of RNA hairpin loops and helices', *J. Biomol. Struct. Dyn.*, Vol. 16, No. 3, pp.671–682.

Synnott, N.C., Bauer, M.R., Madden, S., Murray, A., Klinger, R., O'Donovan, N., O'Connor, D., Gallagher, W.M., Crown, J., Fersht, A.R. and Duffy, M.J. (2018) 'Mutant p53 as a therapeutic target for the treatment of triple-negative breast cancer: Preclinical investigation with the anti-p53 drug, PK11007', *Cancer Lett*., Vol. 414, pp.99–106.

Wang, G. and Fersht, A.R. (2017) 'Multisite aggregation of p53 and implications for drug rescue', *Proc. Natl. Acad. Sci. USA*., Vol. 114, pp.E2634−E2643.

Wang, J., Wolf, R.M., Caldwell, J.W., Kollman, P.A. and Case, D.A. (2004) 'Development and testing of a general amber force field', *Journal of Computational Chemistry*, Vol. 25, No. 9, pp.1157–1174.

Ylilauri, M. and Pentikäinen, O.T. (2013) 'MMGBSA as a tool to understand the binding affinities of filamin–peptide interactions', *Journal of Chemical Information and Modeling*, Vol. 53, No. 10, pp.2626–2633.

Yu, X., Vazquez, A., Levine, A.J. and Carpizo, D.R. (2012) 'Allele-specific p53 mutant reactivation', *Cancer Cell*, Vol. 21, No. 5, pp.614–625.

Zhou, X., Hao, Q. and Lu, H. (2019) 'Mutant p53 in cancer therapy-the barrier or the path', *J. Mol Cell Biol*., Vol. 11, No. 4, pp.293–305.